# Magnetization reversal and interlayer coupling in magnetic tunneling junctions

B. D. Schrag,[a] A. Anguelouch, and Gang Xiao
*Department of Physics, Brown University, Providence, Rhode Island 02912*

P. Trouilloud, Yu Lu, and W. J. Gallagher
*IBM T.J. Watson Research Center, Yorktown Heights, New York 10598*

S. S. P. Parkin
*IBM Almaden Research Center, San Jose, California 95120*

We have studied the switching properties of micron-scale magnetic tunnel junctions in two-dimensional magnetic fields. We present data on interlayer magnetic coupling for multiple samples. We interpret these data as the sum of a magnetostatic and a Néel coupling contribution. The data are presented as functions of layer structure. In addition, we have extracted information about interface roughness. We have also studied the area of switching critical curves as a function of device geometry. © *2000 American Institute of Physics.* [S0021-8979(00)25708-3]

While there have been many studies on magnetic tunneling junctions (MTJs),[1–4] only recently has there been work involving the response of MTJs to two-dimensional magnetic fields.[5,6] Such work is valuable in a technological sense, due to the design ideas regarding magnetic random access memory devices.[4] In addition, study of two-dimensional magnetic switching provides information about micromagnetic and structural properties of MTJs. Magnetic critical ''asteroid'' curves are valuable because they can be directly compared to the Stoner–Wohlfarth model for a single-domain particle to give information about domain structure effects. In addition, asteroid data can be more reliable than one-dimensional results, especially when it comes to interlayer coupling effects. Finally, because consistent fabrication of a clean, uniform tunneling barrier is arguably the most difficult step in fabrication of MTJs, any information regarding the quality of tunneling barriers is invaluable. In this work, we study two-dimensional (2D) magnetic switching in micron-scale MTJs and magnetic interactions between layers. By studying magnetic coupling between magnetic layers adjacent to the barrier, we are able to glean quantitative information about the interface roughness.

Our MTJs were grown via sputtering and patterned using electron beam lithography, as described elsewhere.[3,7] A schematic of the sample is shown in Fig. 1(a). Many junctions on two wafers were studied. These samples were identical in layer structure except for the thickness of the barrier and bottom pinned (P2) layers. The layer sequence with thicknesses in angstroms of sample I is: Si(100) substrate / 50 Ta / 250 Al / 40 $Ni_{60}Fe_{40}$ / 100 FeMn / 60 Co / 7 Ru / 30 Co / 11 $Al_2O_3$ / 75 $Ni_{60}Fe_{40}$ / 250 Al / 75 Ta. The Ta and Al layers serve as buffers to shield the active inner layers, while the 40 Å NiFe ''seed'' layer facilitates growth of a clean, epitaxial sample. The Ru and FeMn layers are inserted to control the magnetic properties of the pinned layers.[3,6] Sample II has a thinner barrier layer (7 Å) and a thinner bottom pinned layer (50 Å). Magnetic tunneling occurs between the free NiFe layer and the Co (P1) layer, which are adjacent to the $Al_2O_3$ barrier on either side. Each patterned chip contains several hundred junctions of various shapes and sizes. We studied rectangular samples with areas between 4 and 128 $\mu m^2$ and aspect ratios ranging from 1:1 to 16:1.

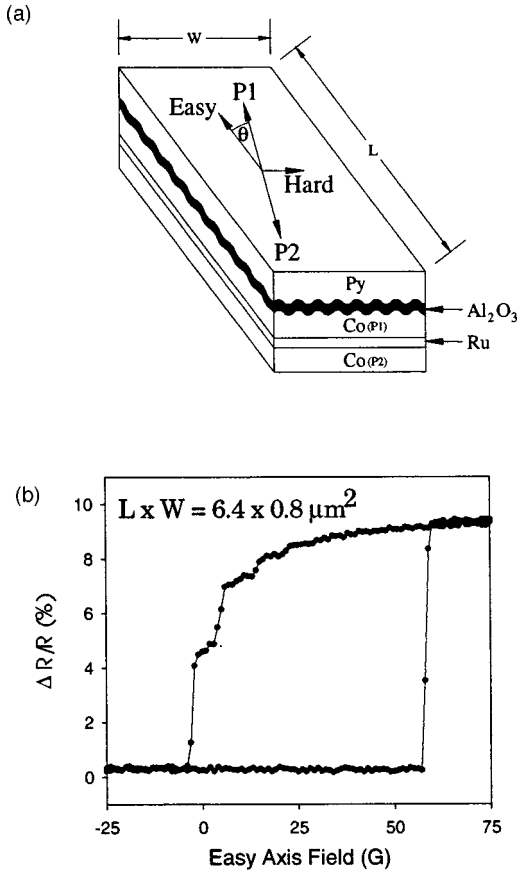


FIG. 1. (a) Schematic of MTJ layer structure. P1 and P2 refer to the top and bottom pinned layers, respectively. (b) Sample hysteresis loop for junction with dimensions $0.8\times6.4$ $\mu$m, with zero applied hard-axis field.

[a]Electronic mail: schrag@barus.physics.brown.edu

 

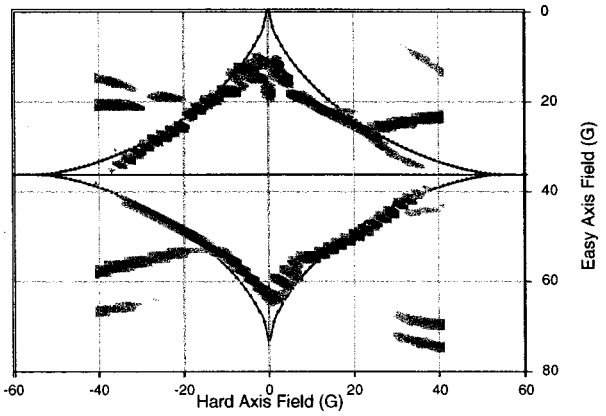


FIG. 2. Sample experimental critical asteroid curve. Darker regions indicate higher probability of switching. The solid black line is a theoretical S–W fit to the data.

The magnetoresistance (MR) of the MTJ samples was measured on a probe station equipped with magnets providing a 2D field (see Ref. 6). For each sample hundreds of MR hysteresis loops along the easy axis were recorded at a fixed hard-axis field. The hard axis field was then incremented and the process repeated. For each MR loop, two switching fields were recorded. These points were plotted in a 2D field space to give the so-called asteroid curve[8] of each sample. One such curve is shown in Fig. 2. The most darkly shaded areas indicate regions of highest switching probability. The theoretical shape of this critical curve for a single-domain particle with uniaxial anisotropy is given by the Stoner–Wohlfarth (S–W) model.[9] While the S–W model predicts a curve centered at the origin of field space, the actual asteroids are generally offset from the origin in both directions.[6,10] In addition, experimental asteroids[5,6] tend to be longer along the hard axis than the easy axis, different from the S–W model prediction of equal critical fields along both directions. In our analysis, we fit experimental critical curves to the S–W model by introducing adjustable parameters which account for these discrepancies: easy-and hard-axis offset fields and a dimensionless constant which measures the compression of the asteroid along the easy axis relative to the hard axis. In Fig. 1, the solid line shows the final result of this fitting process.

We first focus on the offset of the origin of critical curves, which is caused by magnetic interactions between the free and pinned magnetic layers. Two mechanisms contribute to this offset. First, the uncompensated magnetic poles at both ends of the pinned layer create a nonuniform field in the free layer. This magnetostatic coupling appears to scale roughly inversely with the length of the pinned layer. There is also a weak width dependence (see Ref. 6), which we ignore in this article. We express this coupling field, $H_M$, as

$$H_M = B/L, \tag{1}$$

with $B$ an adjustable constant dependent on sample structure. Second, the free layer will also experience the so-called Néel ''orange peel'' coupling[11] through the tunneling barrier and

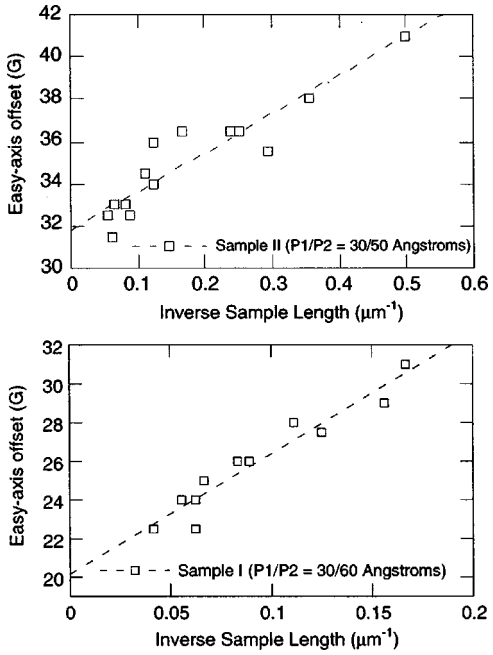


FIG. 3. Easy-axis offset field vs inverse junction length for each sample. The slope of the straight lines gives the $B$ constant, and the intercept on the field axis is the Néel coupling field, $H_N$ [see relation (1) and (2)].

due to the roughness of the interfaces. Independent of sample dimensions, this effect depends on several material parameters as

$$H_N = \frac{\pi^2}{\sqrt{2}}\left(\frac{h^2}{\lambda t_F}\right) M_S \exp(-2\pi\sqrt{2}t_s/\lambda), \tag{2}$$

where $h$ and $\lambda$ are the amplitude and wavelength of the interface roughness, $t_s$ and $t_F$ the thicknesses of the tunneling barrier and free layer, respectively, and $M_S$ is the saturation magnetization of the pinned layer. Equation (1) assumes a sinusoidal interface roughness as an approximation. The net offset field is $H_{\mathrm{OFF}} = H_M + H_N$, which is plotted against $1/L$ for two series of junctions in Fig. 3. The data give straight lines, indicating good agreement with Eqs. (1) and (2). The slope and intercept of these straight lines give measures of magnitudes of the magnetostatic and Néel couplings, respectively. From data fitting we have extracted $B$ and $H_N$ for each series of sample. These values are given in Table I together with sample dimensions for each series.

It can be seen from the sample structure that the pinned Co layer near the barrier tends to bias the free layer antiferromagnetically, whereas the other bottom Co layer tends to do so ferromagnetically. Because the overall coupling due to both Co layers is ferromagnetic in nature, it is clear that the

TABLE I. Structural parameters and interlayer (magnetostatic and Néel) coupling constants for two series of magnetic tunnel junctions with different pinned layer thickness.

| Sample ID | Barrier thickness (Å) | P1 thickness (Å) | P2 thickness (Å) | $B$ ($\mu$m-G) | $H_N$ (G) |
|---|---|---|---|---|---|
| I | 14.3 | 30 | 60 | 56 | 19 |
| II | 9.1 | 30 | 50 | 17 | 31 |

bottom pinned layer dominates this coupling. This result, which is explained by the larger thickness of the bottom pinned layer, is also reproduced by our computer simulations. For the two series of samples listed in Table I, the top pinned layer is kept at 30 Å, but the thickness of the bottom pinned layer is different (50 and 60 Å). Table I shows that the thinner bottom layer does lead to a weaker coupling or a smaller $B$ constant. This is also in agreement with theory, although simulations have predicted a larger value for $B$ than was measured experimentally. It is noted that our simulations assume a single domain free layer and equate the offset field to the unweighted average dipolar field over the area of the free layer. In reality, these assumptions represent a substantial degree of simplification. Nevertheless, the sensitivity of $B$ to the thickness the pinned layers can be used to design MTJs with a diminishing field offset and symmetrical asteroid.

Table I also lists the fitted Néel coupling field ($H_N$) vs. barrier thickness. The samples with a thinner barrier have a larger $H_N$, as predicted by relation (2), which shows an exponential thickness dependence. Assuming that each sample has similar roughness characteristics, applying to relation (2) parameters of $H_N$ and sample dimensions ($t_s$ and $t_F$) allows us to extract values for the wavelength (94 Å) and magnitude (7.3 Å) of the interface roughness. These values are reasonable when compared with roughness estimation from transmission electron microscopy cross-sectional images of the barrier regions. We believe that this method of quantifying roughness is useful in optimizing the quality of barriers.

Finally, we address the issue of asteroid size. The S–W model predicts an asteroid which is symmetric along the easy- and hard-axis field directions and whose area scales as $(2H_K/M_S)^2$, where $H_K$ is the critical field of the layer of interest. For rectangular samples with a high aspect ratio, $H_K$ due to shape anisotropy scales inversely with the sample width ($w$),

$$H_K = 4\pi M_S t_F / w. \tag{3}$$

Therefore, we should see the area of the critical curve scales as $w^{-2}$. We have measured the area of critical curves for many samples with varying aspect ratios. These areas are plotted versus junction width in Fig. 4 with a log–log scale. We find that the area scales as a power law in junction width, i.e., $S = Cw^{-1.4}$, where $C$ is a constant which depends only on the sample aspect ratio. Solid lines in Fig. 4 are fits to the data with this form. Samples with differing aspect ratios are seen to lie on parallel lines. The discrepancy between the theoretical power-law of $w^{-2}$ and the experimental $w^{-1.4}$ is likely caused by the multidomain structure in our samples. Micromagnetic simulation should shed light on this $w^{-1.4}$ scaling of the area.

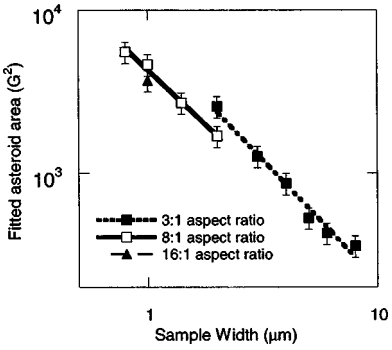


FIG. 4. Asteroid area ($S$) as a function of sample width. The two solid lines are power-law fits ($S = Cw^{-1.4}$) to the data for rectangular junctions with aspect ratios 3:1 and 8:1.

In summary, we have demonstrated that study of critical asteroid curves can provide a great deal of information regarding interlayer coupling strength and domain-structure effect in MTJs. We have separated the coupling field into a magnetostatic component inversely proportional to the length of a junction and a Néel term due to interface roughness. A comparison of these terms for differing layer structures has shown our data to be consistent with theory. We were able to characterize the interface roughness near the barrier region of the junctions. We have also shown that the area of critical curves scales according to a new power law in the junction width.

This work was supported by National Science Foundation Grant Nos. DMR-9701579 and DMR-9414160, and partially by Defense Advanced Research Projects Agency.

[1] J. S. Moodera, L. R. Kinder, T. M. Wong, and R. Meservey, Phys. Rev. Lett. **74**, 3273 (1995); J. Appl. Phys. **79**, 4724 (1996).
[2] N. Tezuka and T. Miyazaki, J. Appl. Phys. **79**, 6262 (1996); J. Magn. Magn. Mater. **139**, L231 (1995).
[3] W. J. Gallagher *et al.*, J. Appl. Phys. **81**, 3741 (1997).
[4] S. S. P. Parkin *et al.*, J. Appl. Phys. **85**, 5828 (1999).
[5] Y. Lu *et al.*, J. Appl. Phys. **85**, 5267 (1999).
[6] A. Anguelouch, B. D. Schrag, G. Xiao, R. Wanner, P. Trouilloud, Y. Lu, W. J. Gallagher, and S. S. P. Parkin (unpublished).
[7] S. A. Rishton *et al.*, Microelectron. Eng. **35**, 249 (1997).
[8] J. C. Slonczewski, Research Memo. 003.111.224, IBM Research Center, Poughkeepsie, NY (1956), unpublished.
[9] E. C. Stoner and E. P. Wohlfarth, Philos. Trans. R. Soc. London, Ser. A **240**, 599 (1948).
[10] K.-S. Moon, R. E. Fontana, Jr., and S. S. P. Parkin, Appl. Phys. Lett. **74**, 3690 (1999).
[11] L. Néel, Comptes. Rendus **255**, 1676 (1962).